RADIATIVE HEATING OF VEHICLES ENTERING THE EARTH'S ATMOSPHERE

By Bradford H. Wick

Ames Research Center
Moffett Field, Calif., U.S.A.

Presented to the Fluid Mechanics Panel
of Advisory Group for Aeronautical
Research and Development

Brussels, Belgium
April 3-6, 1962

NATIONAL AERONAUTICS and SPACE ADMINISTRATION
WASHINGTON

ABSTRACT

33189

This paper considers the problem of calculating the equilibrium radiative heating of vehicles entering the Earth's atmosphere at velocities up to twice satellite velocity, with particular attention given to the cases of manned vehicles returning from trips to the Moon and Mars. Information and methods pertinent to the calculation of equilibrium radiative heating are presented and discussed. Numerical results are presented for evaluating stagnation-point heat flux and heat-flux distributions for spherical-segment noses for wide ranges of velocity and altitude. The results are for constant-energy shock layers of hot air which does not absorb radiation. The influence on stagnation-point radiative heat flux of absorption of shock-layer radiation, and the loss of shock-layer energy caused by the radiation is discussed and illustrated. Finally, calculated values of stagnation-point radiative heat flux and total heat are presented for manned lunar and Mars vehicles, and are compared with corresponding values for convective heating.

Author

CONTENTS

CONTENTS - Concluded

FIGURE TITLES

NOTATION

A	area of base of spherical segment nose, $\pi D^2/4$
B_ν	Planck black-body distribution function
C_D	drag coefficient, $\frac{2 \text{ drag}}{\rho_\infty V_\infty^2 A}$
D	diameter of base of spherical segment nose
E_t	total energy radiated per unit time per unit volume of hot air
h	enthalpy of shock layer
k_c	factor for convective heating
k_s	shape factor for radiative heating
l	distance from surface of nose to point in shock layer, measured in direction normal to surface
l_s	distance from surface of nose to shock, measured in direction normal to surface
L_{abs}	characteristic length for absorption
L_{dec}	characteristic length for decay
L/D	lift-drag ratio
$(L/D)_i$	lift-drag ratio at entry
n	exponent
p	pressure
p_∞	free-stream pressure
p_s	pressure immediately behind shock
p_{s_o}	pressure immediately behind normal part of shock
$\dot{q}_{c_o}$	convective heat flux at stagnation point
$\dot{q}_r$	local radiative heat flux
$\dot{q}_{r_o}$	radiative heat flux at stagnation point
R	nose radius
R_s	shock radius

s	distance along surface of nose, measured from center line of nose
s_e	distance along surface of nose to edge of nose, measured from center line of nose
t	dummy variable of integration for τ
T	temperature in shock layer
T_s	temperature immediately behind shock
T_{s_o}	temperature immediately behind normal part of shock
V	velocity in shock layer
V_∞	free-stream velocity, or vehicle velocity
W	vehicle weight
x	distance behind normal shock
α	angle of attack
β	angle between normal to surface at stagnation point, and ray between radiating volume and stagnation point
δ	shock standoff distance
δ_o	shock standoff distance at stagnation point
μ	absorption coefficient
$\bar{\mu}$	mean absorption coefficient, $\dfrac{\int_o^\infty \mu_\nu B_\nu \, d\nu}{\int_o^\infty B_\nu \, d\nu}$
ν	frequency
ξ	$\cos \beta$
ρ	density of air in shock layer
ρ_o	atmosphere density at standard conditions
ρ_∞	local atmosphere density
ρ_s	density of air immediately behind shock
ρ_{s_o}	density of air immediately behind normal part of shock

σ	Stefan-Boltzmann constant
τ	optical thickness
τ_w	optical thickness at wall

RADIATIVE HEATING OF VEHICLES ENTERING THE EARTH'S ATMOSPHERE

By Bradford H. Wick*

National Aeronautics and Space Administration
Ames Research Center
Moffett Field, Calif.

1. INTRODUCTION

This paper is concerned with the problem of predicting the radiative heating of vehicles entering the Earth's atmosphere at velocities up to twice satellite velocity. Methods and information pertinent to the prediction of equilibrium radiative heating are summarized and applied. The presentation is divided into the following four topics: (1) a general description of the several cases of equilibrium radiative heating that can occur for various vehicle and flight conditions, (2) stagnation-point heat flux and heat-flux distributions for one particular radiative heating case, (3) stagnation-point heat flux for the several radiative heating cases, and (4) the stagnation-point heat flux for specified manned vehicles entering the Earth's atmosphere on return trips from the Moon and Mars. Values of radiative heat flux are compared with corresponding values of laminar convective heat flux.

2. DESCRIPTION OF THE SEVERAL CASES OF EQUILIBRIUM RADIATIVE HEATING

Two important cases of radiative heat transfer from equilibrium shock layers can be described with the aid of Fig. 1. The case illustrated on the left is that for a shock layer which is assumed to have constant total energy throughout the layer, and which does not absorb any of the radiation. For this case, the radiation intensity is

---

*Research Scientist

constant in the equilibrium region, as depicted by the small radiating volumes in the shock layer. The temperature is also constant in the equilibrium region, as shown by the temperature profile for the shock layer. This case of radiation from a constant-energy, nonabsorbing shock layer is valid whenever the radiant energy flux from the shock layer is small compared to the energy flux of the flow entering the shock layer. If the radiant energy flux is relatively large, one encounters the case that is illustrated on the right side of Fig. 1. The flux of radiant energy from the air as it flows toward the stagnation point results in a decay of shock-layer energy, and a consequent drop in shock-layer temperature. This radiation cooling in turn attenuates the intensity of radiation, as depicted by the radiating volumes in the shock layer, and thus slows down the rate of decay of shock-layer energy and temperature.

In addition to these two cases of equilibrium radiative heat transfer from nonabsorbing shock layers, there are two parallel cases for absorption. Thus, from considerations of shock-layer energy decay and radiation absorption, the following four cases of equilibrium radiative heat transfer can be identified: (1) no decay or absorption, (2) decay only, (3) absorption only, and (4) decay and absorption.

The velocity-altitude regions in which these four cases of equilibrium radiative heating are important depend upon the specific vehicle size, shape, and angle of attack. A procedure for determining the regions for specific vehicle conditions is given in a subsequent section of the paper. A qualitative indication of the relative extents and locations of the regions is provided in Fig. 2. Along the top of the

figure, arrows show the entry velocities for Earth satellites, and for vehicles returning from trips to the Moon and Mars. A boundary between equilibrium and nonequilibrium radiative heating is also shown. For quantitative definition of this boundary, use can be made of the information on nonequilibrium radiative heating presented by Canning (1) during a previous session of this meeting. The important general fact brought out by this figure is the increasing importance of the decay of shock-layer energy and the absorption of the radiation with increasing entry velocity.

3. EQUILIBRIUM RADIATIVE HEAT FLUX WITHOUT DECAY OR ABSORPTION

3.1 Stagnation-Point Flux

The geometry and equations used in calculating the stagnation-point heat flux are shown in Fig. 3. The sketch on the left illustrates a spherical segment wall surrounded by a spherical segment shock. For purposes of clarity, the shock standoff δ_o is shown exaggerated with respect to the wall radius. The portion of the shock layer that radiates to the stagnation point is designated by shading. An elemental volume of shock-heated air is shown radiating to the stagnation point. The total radiative heat flux at the stagnation point is obtained by summing up the contributions of all the elemental volumes in the shaded portion of the shock layer. A frequently used approximation in carrying out the summation is to replace the actual spherical segment shock layer by a plane layer with a thickness equal to the shock standoff, and use stagnation temperature and density. If it is further assumed that the

wall does not reflect or emit energy, the equation for the stagnation point heat flux can then be written as shown on the upper right side of the figure. The quantity $E_t/2$ represents one-half of the total radiant energy flux from each unit volume. The factor of 1/2 is to account for the fact that half the total radiant energy leaves each side of a thin shock layer. If the plane layer approximation is used, the stagnation-point heat flux is equal to the product of $E_t/2$ and the shock standoff δ_o. The plane-layer approximation has the advantage of great simplicity and also the merit of being reasonably accurate for practical cases. There are two reasons for this result. First, the actual shock layer approaches a plane layer because the shock standoff distance is small compared to the shock radius of curvature. Second, in those portions of the shock layer which contribute most of the heat flux to the stagnation point, the temperature and density do not differ significantly from the stagnation values.

A refinement that one can make to the plane-layer approximation is to perform the integration over only the spherical segment. The final equation for the stagnation-point flux differs from the plane-layer equation by a factor k_s which can be termed the shock shape factor. We see from this equation, that the radiative heat flux to the stagnation point of a body depends upon the radiant energy flux per unit volume of shock-heated air, the shock standoff distance, and the shock shape factor. Each of these quantities will be considered in turn.

Values of $E_t/2$ obtained from the work of Kivel and Bailey (2) are shown in Fig. 4 in the form of curves of constant $E_t/2$ on an altitude-velocity chart. As pointed out by Kivel (3), this form is convenient

for making rapid estimates of stagnation point heat flux for particular entry trajectories. These values of $E_t/2$ were recently compared with the values that can be determined from the absorption coefficients for air that were calculated by Meyerott, et al. (4). The two sets of values were in reasonably good agreement except at the higher velocities. Here the values from Kivel and Bailey were generally higher by a factor of 2. Kivel (3) discussed the uncertainty in the values given by Kivel and Bailey at the higher velocities, and noted that they were probably high by a factor of 2. Until such time, however, that the differences can be resolved by experiment, it appears preferable to take the more conservative approach and use the higher values.

Calculated values of shock standoff distances for spherical-segment nose shapes at zero angle of attack are summarized in Fig. 5. The values are shown in the form of the ratio of shock standoff to nose radius as a function of the ratio of free-stream density to the density behind the normal part of the shock. By way of explanation, the nose with a value of $R/D = 0.5$ is a hemisphere and the $R/D = 2.0$ nose is a spherical segment terminating at 14.5° from the stagnation point. The calculations were made by a method developed by Kaattari at Ames Research Center. As Kaattari has shown (5), the method gives results in good agreement with experimental results for both perfect and real-air cases. Noted on the figure is the range of density ratios for the range of flight velocities and altitudes of interest in radiative heating calculations. A good average value of the ratio of shock standoff to nose radius is 0.045.

The effect of angle of attack on shock standoff distance at the stagnation point is summarized in Fig. 6 for various spherical segment nose shapes. The results are presented in the form of the ratio of the standoff distance at angle of attack to the corresponding value at zero angle of attack. Again, these results were calculated by use of Kaattari's method, and again the method has been shown to give results in good agreement with experimental results. All the curves terminate at the dotted line designated as the limit of the theory. This limit is defined by the angle of attack at which the edge of each nose shape becomes parallel to the free stream. It is interesting to note that for all of the nose shapes considered, the shock standoff ratio for this limiting angle of attack is about 0.43. This means that from the standpoint of radiative flux each capsule at this limit has an effective nose radius equal to 0.43 of its geometric radius. From the standpoint of convective flux the effective nose radius is also smaller, but by a slightly different amount than for the radiative flux.

The results for the shock shape factor are summarized in Fig. 7. It was found to be a function of density ratio only for the ranges of nose shape and angle of attack shown on the figure. For convenience, the radiative heat-flux equation has been repeated from the earlier figure. The shape factor does not differ much from 1.0, and in view of the uncertainties in the values of $E_t/2$ one would be justified in using a value of 1.0. If the factor is taken into account, however, a value of 0.84 appears to be a good average value to use for the density ratio range of interest in the radiative heat-flux calculations.

With the information in Figs. 4 through 7, one can make rapid estimates of equilibrium radiative heat flux for the stagnation points of a number of different nose shapes for wide ranges of velocity and altitude. As indicated previously, however, there are limits to the applicability of the results that depend upon the vehicle nose radius. Within the limits of applicability, the stagnation-point radiative heat flux bears the well-known direct proportionality to nose radius as a result of the direct proportionality between shock standoff distance and nose radius. Values of equilibrium stagnation-point radiative heat flux of a hemisphere have previously been published by Yoshikawa and Wick (6); the values given therein will differ slightly from values calculated from the data presented in this paper because of slight differences in shock standoff distance.

3.2 Heat-Flux Distributions

In calculating distributions of radiative heat flux, detailed calculations must be made of the local temperatures and densities in the shock layers. Once these values have been determined one can determine local values of $E_t/2$ from tables or plots of $E_t/2$ as a function of temperature and density. (See (2) and (3) for values of $E_t/2$ presented in these forms.) The next step is a lengthy summation of the radiation from all the local elemental volumes.

As pointed out by de l'Estoile and Rosenthal (7), it is possible to resort to the plane-layer approximation, and thus reduce the number of calculations without introducing significant errors. The application of the approximation differs, however, from that used for the stagnation

point. As shown by the sketch presented in Fig. 8, one has to divide the shock layer into a number of plane layers. This procedure is necessary because of variations in temperature and density between the shock and the wall, and the consequent variation in the radiant energy flux per unit volume. One can then employ the simple integral equation shown at the top right of the figure to obtain the local radiative heat flux.

Typical variations in temperature, density, and radiant energy flux are shown by the plots on the right of Fig. 8; the quantities are normalized with respect to conditions behind the normal part of the shock wave. The most striking feature about these distributions is the rather sizable deviation of the ratio of radiant energy flux from unity, compared to the rather minor deviations of the corresponding temperature and density ratios. For example, the radiant energy flux near the wall is about 65 percent of the value in the stagnation region, whereas the temperature is about 97 percent of the comparable value in the stagnation region. This large change is primarily the result of the temperature change, small though it is; the radiant energy flux varies approximately as the eleventh power of temperature, and only as the 1.3 power of density. This strong effect of temperature places stringent requirements on the method of calculating the shock-layer temperatures.

The following procedures were employed in calculating the many shock-layer temperatures and density distributions employed in this paper. The equilibrium values of temperatures and densities at various points immediately behind the shock were determined from the normal-shock properties of air given by Hochstim (8) and by the use of oblique

shock theory. The shock-layer temperatures and densities at the wall were determined by an unpublished method developed by Kaattari of the Ames Research Center; the accuracy of the method has been verified by comparison of calculated pressure distributions with those measured on several spherical-segment models at supersonic and hypersonic speeds. For intermediate points in the shock layer, a linear interpolation was used between the shock and the wall. This procedure was selected on the basis of the examination of the results of calculations by the stream-tube method of Maslen and Moeckel (9) of several blunt-body shock layers for real-air conditions, and the results of calculations made by Fuller, of the Ames Research Center, of hemisphere shock layers for perfect gas conditions (see (10)).

The results of the calculations of radiative heat-flux distributions for zero angle of attack are summarized in Fig. 9. The ratio of the local heat flux to the stagnation-point heat flux is plotted as a function of the ratio of local position to the edge position. The solid curves show the mean distributions for the various noses for the ranges of velocity and altitude indicated. (For values of R/D of 1.0 and 2.0 the velocity range extends down to 8 km/sec.) The bands show the spread in values for the same ranges of velocity and altitude. As a reminder when the distributions are examined, the nose with an R/D = 0.5 is a hemisphere, and the R/D = 2.0 nose is a spherical segment terminating at 14.5° from the stagnation point; thus the lower the value of R/D, the less blunt the nose. As might be expected from considerations of the effect of bluntness on the variations of temperature and density away from the stagnation point, the less blunt the nose, the more

rapidly the radiative heat flux decreases from the stagnation-point value.

Insofar as is known, only one radiative heat-flux distribution has been available in the unclassified literature. This is a distribution presented by de l'Estoile and Rosenthal (7) for an essentially complete hemispherical nose. The calculations were made for a velocity and altitude which were lower than those considered here. The decrease in the radiative heat flux was less rapid than that shown by the present calculations. The probable explanation for the difference is that the radiant energy rate is less strongly affected by variations in temperature and the temperature changes less rapidly with shock inclination for the lower ranges of velocity and altitude.

The radiative heat-flux distribution for the R/D = 1.0 nose is compared with corresponding laminar convective heat-flux distribution in Fig. 10. The radiative heat flux decreases more rapidly away from the stagnation point than does the laminar convective heat flux. For example, the radiative heat-flux ratio is approximately 0.2 at the edge of the nose compared to the convective heat-flux ratio of about 0.8. The difference would be even greater for the hemisphere.

The effect of angle of attack on the distribution of radiative heat flux is illustrated in Fig. 11. The results are for the vertical plane of the R/D = 1.0 nose for angles of attack of 0°, -15°, and -30°. The local values of heat flux are normalized with respect to the stagnation value for zero angle of attack. Thus the curves show not only the change in shape of the distribution with angle of attack but also the change in level. The reference point for the ratio s/s_e is the center

line of the nose. The locations of the stagnation point are indicated by tick marks. (The velocity and altitude ranges of applicability of these distributions are the same as those previously indicated on Fig. 9.) Large variations in radiative heat flux are evident for all three angles. For the -30° angle condition, peak heating does not occur at the stagnation point but occurs at a point downward from the stagnation point. This result may appear surprising in view of the fact that the radiation intensity immediately behind a shock wave is extremely sensitive to the normal component of velocity, and hence should decrease rapidly with shock-wave inclination. The radiation intensity does decrease with increasing distance from the stagnation region, but initially the effect on the heat flux to the wall is more than offset by the effect of the growing shock-layer thickness.

4. EQUILIBRIUM RADIATIVE HEAT FLUX WITH DECAY AND ABSORPTION

4.1 General Considerations

In accounting for the effects of decay and absorption on the radiative heat flux to an entry vehicle, the basic radiative heat-flux equations must be coupled with the appropriate equations for the air flow. One then encounters rather complex and formidable integro-differential equations even for simple one-dimensional flow geometries. In view of this situation, it is not surprising that solutions for three-dimensional hypersonic shock layers are not yet available in the literature. At the present time one must make use of one-dimensional flow results in considering the effects of decay and absorption on the radiative heat flux to entry vehicles.

The work of Goulard and Goulard has been very helpful in this regard ((11) and (12)). They apparently were the first to give serious attention to the interactions between the various energy transport processes in high-temperature gas flows. They have extended the classical equations for radiative energy transfer available from the work of astrophysicists ((13) and (14)) to one-dimensional flows of chemically reacting gases and have included the influence of absorbing and radiating walls. Solutions have been provided for the Couette flow of a radiating and chemically reacting gas, and for a one-dimensional layer of radiating and conducting gas between walls of arbitrary radiative properties.

Recently, Yoshikawa and Chapman of the Ames Research Center have obtained a relatively simple solution for the case of high-temperature air emitting and absorbing radiation behind a one-dimensional shock wave in hypersonic flow. The following assumptions were used in their analysis:

(a) Gray-gas radiation with local thermodynamic equilibrium of the radiation and the gas properties behind the shock wave.

(b) Negligible absorption upstream of the shock wave of the radiation from the region downstream of the shock wave.

(c) Transparent shock front (zero reflection of radiation passing upstream through the shock front).

(d) Black body wall (hypothetical) emitting a radiative flux that is very small compared to that from the shock layer.

(e) Negligible heat transfer by thermal conduction and convection compared to that by radiation.

(f) Heat flux at a black body wall in a flow with shock standoff distance δ is the same as that in a one-dimensional hypersonic flow wherein all downstream radiation is absorbed at a distance δ behind the shock wave.

Numerical results have been obtained for the distribution of upstream and downstream radiative heat flux. Air pressures up to 10^3 atmospheres and temperatures to 15,000° K were considered. The results of the analysis are employed in the present paper in examining the effects of decay and absorption on the radiative heat flux, and in estimating stagnation-point radiative heat flux for a specific entry vehicle. The basic equations solved and some relations for characteristic lengths in the problem are presented, and are then followed by some illustrative results. The estimates of stagnation-point heat flux are presented in the subsequent section of the paper.

4.2 Basic Equations for Radiative Heat Flux

The following basic equations were derived by combining the basic radiative heat-transfer equations with the equations describing the fluid dynamics of the air flow behind a hypersonic normal shock wave and employing the aforementioned assumptions:

Continuity

$$d(\rho V) = 0$$

Momentum

$$dp + V\,dV = 0$$

Energy

$$\rho_\infty V_\infty dh = d\dot{q}_r$$

Radiant energy transfer

$$d\dot{q}_r = \left\{ 4\sigma T^4 - \int_0^{\tau_w} 2\sigma T^4 E_1 |t-\tau| dt \right\} d\tau$$

where the integro-exponential function E_1 (see (12) and (13)) is defined by

$$E_n(t) = \int_0^1 \xi^{n-2} e^{-t/\xi} d\xi$$

and τ is the optical path length defined by

$$\tau = \int_0^x \bar{\mu}\, dx$$

The quantity $\bar{\mu}$ is the Planck mean absorption coefficient for an optically thin layer of gas (see notation section), and can be expressed in terms of $E_t/2$ by the following relation:

$$\bar{\mu} = \frac{(E_t/2)}{2\sigma T^4}$$

One can also treat the case of a one-dimensional radiating but nonabsorbing layer behind a hypersonic normal shock. In this case the equations for the fluid flow are coupled with the following equation for the radiant energy transfer:

$$d\dot{q}_r = 4\sigma T^4 d\tau$$

Solutions of this case provide some useful answers as will be discussed later.

The following equations for the radiation from a one-dimensional layer to a cold absorbing wall are of interest in showing the influence of various assumptions regarding the shock layer:

Absorbing, anisothermal layer

$$\dot{q}_r = \int_0^{\tau_w} 2\sigma T^4 E_2(\tau_w - t)dt$$

or

$$\dot{q}_r = \int_0^{\pi/2} \int_0^{\tau_w} 2\sigma T^4 \exp\left(\frac{\tau - \tau_w}{\cos \beta}\right) \sin \beta \, d\beta \, d\tau$$

Absorbing, isothermal layer

$$\dot{q}_r = 2\sigma T^4 \left[\frac{1}{2} - E_3(\tau_w) \right]$$

or

$$\dot{q}_r = 2\sigma T^4 \left[\frac{1}{2} - \int_0^{\pi/2} \exp\left(\frac{-\tau_w}{\cos \beta}\right) \cos \beta \sin \beta \, d\beta \right]$$

Nonabsorbing, anisothermal layer

$$\dot{q}_r = \int_0^{\tau_w} 2\sigma T^4 d\tau$$

or

$$\dot{q}_r = \int_0^{\pi/2} \int_0^{\tau_w} 2\sigma T^4 \sin \beta \, d\beta \, d\tau$$

Nonabsorbing, isothermal layer

$$\dot{q}_r = 2\sigma T^4 \tau_w = (E_t/2)\delta$$

The absorbing, anisothermal layer is that treated by Yoshikawa and Chapman for one-dimensional hypersonic flow. The equation for the absorbing isothermal layer was derived by Goulard and Goulard (12)

and Kennet and Strack (17). The equation was evaluated by Kennet and Strack for the case of no flow, using the tables for the integro-exponential functions given in (13). The equation for the nonabsorbing isothermal layer is identical to that previously given in Fig. 3.

4.3 Relations for Characteristic Lengths

In studying the effects of decay and absorption, it is useful to employ the concept of a characteristic length L_{dec} for the decay and L_{abs} for absorption. The magnitude of the shock standoff distance δ relative to these characteristic lengths provides an indication of the velocity-altitude regions in which the two effects are important. Goulard has presented and discussed numerical values for these lengths ((12), (15), and (16)). The relations for the two characteristic lengths are

$$L_{dec} \equiv \frac{(1/2)\rho_\infty V_\infty^3}{E_t}$$

and

$$L_{abs} \equiv \frac{1}{2\bar{\mu}}$$

Decay becomes important when

$$\delta \geq 0.1\, L_{dec}$$

and absorption becomes important when

$$\delta \geq 0.1\, L_{abs}$$

4.4 Radiative Heat Flux

The conditions selected for presenting results are a velocity of 15 kilometers per second and an altitude of 57 kilometers (T_{s_o} = 15,000° K, p_{s_o} = 1 atm). Radiative heat-flux values for these conditions are presented in Fig. 12. The values are shown as fractions of the black body limit based on the temperature immediately behind the shock for various shock standoff distances. Values for four shock-layer cases are examined: (1) no decay or absorption, (2) absorption only (using the isothermal approximation, which is physically realistic for very small standoff distances only), (3) decay only (shown by the circles), and (4) decay and absorption combined (obtained from the calculations of Yoshikawa and Chapman). The large decreases in heat flux from the case of no decay or absorption are entirely the result of decay. This is shown by the good agreement between the curve for decay and absorption and the decay-only points, and also by the absorption-only calculations. The shock standoff distance for a 3-meter radius nose at zero angle of attack is about 13.5 centimeters. For this distance the radiative heat flux with decay is about 50 percent of the value for no decay. The value of L_{dec} for this combination of velocity and altitude is about 16 centimeters as indicated by the arrow pointing to the horizontal axis. Thus, the shock standoff distance of 13.5 centimeters is nearly equal to the characteristic distance for decay. The figure also indicates the validity of using a distance equal to 0.1 L_{dec} to define the altitude-velocity region for decay. At this distance (1.6 cm) the effect of decay is just beginning. The situation with respect to L_{abs} is shown

in the inset in the figure. Here the results have been plotted to academically large values of shock standoff distance. The value of L_{abs} is about 130 centimeters, and thus is about 8 times larger than L_{dec}. At the value of L_{abs}, the curve for no absorption or decay reaches the black-body limit based on the temperature immediately behind the shock wave. In contrast, the decay and absorption reaches a level of about 8 percent of the limit. A black-body limit loses most of its significance for a shock layer with large temperature gradients. Also, the use of the isothermal approximation to define the effect of absorption clearly becomes untenable.

As has been noted by Goulard ((15) and (16)), such large amounts of decay of shock-layer energy by radiation affect not only the radiative heat flux to the wall but the convective heat flux as well. This is a consequence of the shock layer being much cooler at the edge of the boundary layer than it would have been had the decay of energy not occurred. The cooling effect should diminish the amount of ionization if the shock layer remains in equilibrium as assumed in the calculation of the radiation cooling. The possibility thus exists that the radiation cooling could significantly reduce the effects of ionization on convective heat flux to be expected at supersatellite velocities. (See (18).)

Radiative heat-flux values were also calculated and compared in the manner just described for a combination of velocity and altitude in the region where both decay and absorption are important for standoff distances of practical interest. These conditions were a velocity of 12.5 kilometers per second and an altitude of 36.5 kilometers (T_{s_o} = 15,000° K, p_{s_o} = 10 atm). Briefly, the results can be summarized in the following

manner. The radiative heat flux for decay and absorption was about 50 percent of the value for no absorption or decay at a shock standoff distance of 4 centimeters (L_{dec} = 6 cm; L_{abs} = 6 cm). The corresponding value predicted for decay alone was about 40 percent, thus indicating coupling between absorption and decay. Absorption traps radiant energy that would otherwise escape from the shock layer.

Effects of decay and absorption of the magnitude just discussed are not likely to occur for manned vehicle entry at speeds up to twice satellite speeds, judging from the results of the heat flux calculations presented in the following section of the paper. Effects of such magnitude are more likely to occur for unmanned vehicles entering the atmosphere at very steep angles.

5. STAGNATION-POINT RADIATIVE HEAT FLUX FOR SPECIFIC ENTRY VEHICLES

5.1 General Conditions

The vehicles considered are manned vehicles for entering the Earth's atmosphere on return trips from the Moon and Mars. The same size, shape, and weight of vehicle were selected in each case. A blunt capsule with hemispherical segment nose with a value of R/D = 1.0, and a diameter of 3 meters was selected. A value of W/C_DA = 250 kilograms per square meter was deemed appropriate.

The trajectories used in the heating calculations were determined on an IBM 7090 computer. Two types of trajectories were considered for each vehicle. One was along the undershoot boundary of the entry corridor using an $(L/D)_i$ of 0.5, and the other was along the overshoot boundary of the entry corridor using an $(L/D)_i$ of -0.5. The concept of an entry

corridor and the definition of its boundaries are discussed at some length by Chapman (19). Briefly, the undershoot boundary is defined by a deceleration limit (10 Earth g in the present case), and the overshoot boundary is defined by the requirement that the vehicle be captured by aerodynamic braking. The greater the corridor depth, the less stringent are the requirements for guidance system accuracy. The corridor depth for the case of the lunar vehicle was about 23 kilometers, and 9 kilometers for the Mars vehicle. A skipping maneuver was used for both entry trajectories in order to provide a maximum range in each case of about 10,000 kilometers. The maximum altitude of the skips was limited to about 120 kilometers. The maneuvering was accomplished by step changes from $L/D = 0.5$ to -0.5 or vice versa. For the nose shape chosen, a value of $L/D = 0.5$ requires an angle of attack of 30°. The entry velocity was taken to be $\sqrt{2}$ times satellite velocity for the lunar vehicle, and twice satellite velocity for the Mars vehicle.

Calculations of stagnation-point heat flux were made not only for the case of equilibrium radiative heat transfer but also, for comparative purposes, for the case of laminar convective heat transfer. The values of laminar convective heat flux were calculated by use of the following simple relation:

$$\dot{q}_{c_o} = \frac{k_c}{R^{0.5}} \left(\frac{\rho_\infty}{\rho_o}\right)^{0.5} V_\infty{}^3 \left[\frac{1 + \frac{1}{(\delta_o/R)_{cap}}}{1 + \frac{1}{(\delta_o/R)_{hem}}}\right]^{0.5}$$

where $k_c = 51$ when $\dot{q}_{c_s}$ is in Kg cal/m^2sec, R is in meters, and V_∞ is in km/sec. The equation is essentially that given by Lees (20) for a hemisphere at hypersonic speed, modified by the ratio in the bracket

to account for the fact that the stagnation-point velocity gradient for a blunt capsule differs from that for a hemisphere. The modification introduced here is based on the correlation between stagnation-point velocity gradient and stagnation-point shock standoff distance that was developed by Traugott (21), and used by Kaattari (5) in his development of a method of predicting shock standoff distances. It is recognized that the equation does not account for the effects of the ionization that would occur in the air after it passes through the shock wave. On this count, the equation would be expected to underpredict the convective heat-flux values for the higher velocity entries. Radiation cooling of the shock layer did not prove to be much of a factor in the present calculations. As previously discussed, the values of $E_t/2$ used in the calculation of radiative heat flux could be too high by a factor of 2 at the higher velocities. The values of radiative heat flux would be too high by the same factor.

Granting that there are uncertainties in the information and methods presently available for calculating both types of heating for the higher entry velocities, it is believed that the following estimates provide a reasonable approximation of the relative severity of the two types of heating for entry velocities up to twice satellite velocity. The aforementioned uncertainties point up the need for much additional research. One can hope that it will be accomplished long before the time arrives for engineering decisions on manned spacecraft for missions to Mars and return.

5.2 Stagnation-Point Heat Flux for Manned Lunar and Mars Vehicles

The calculated values of heat flux for a manned lunar vehicle are presented in Fig. 13. The values are shown as a function of time; the resulting curves for the overshoot trajectory are shown on the left, and those for the undershoot trajectory are shown on the right. Above each set of heat flux curves are values of total radiative and convective heat for the stagnation point. Only in the case of the undershoot entry is the radiative heat flux significant compared to the convective. The peak value of the radiative heat flux is about 40 percent of the convective peak. The radiative heat pulse peaks at about 93 percent of entry velocity and the convective pulse peaks at about 90 percent. The period of the radiative heat pulse is much shorter than that for the convective. As a consequence of both the lower peak and the shorter heating period, the total radiative heat for undershoot is only about 5 percent of the total convective heat. It should be noted that the total convective heat is higher for overshoot than for undershoot. The lower values of convective heat flux for the overshoot case are more than offset by the longer heating period for the overshoot trajectory.

The entry heating results for the case of the manned vehicle returning from Mars are displayed in Fig. 14, in the same manner as that used for the lunar vehicle case. The results for the Mars vehicle are in sharp contrast to those just shown for the lunar vehicle. The peak radiative heat flux is higher than the convective peak for both the undershoot and the overshoot trajectories. It is over a factor of 3 higher for the undershoot trajectory. The total radiative heat is about

the same magnitude as the convective heat for both trajectories. (The peaks for both types of heating occurred at about 93 percent of entry velocity.)

Only in the case of the undershoot trajectory is the peak in the radiative heat flux affected by the decay of shock-layer energy by radiation. For this case, the peak of the radiative heat flux is about 85 percent of that obtained for no decay.

To illustrate the effect of entry velocity, the peak heat-flux values for the lunar vehicle are shown by the circles on Fig. 14; the open circles are for the convective peaks, and the solid circles are for the radiative peaks. Evident from the comparisons is the increasing importance of radiative compared to convective heating as the entry velocity for manned space vehicles is increased. The combined total heat quadruples, as can be seen from a comparison of the values given in Figs. 13 and 14.

In considering the relative importance of the two types of heating, one is also interested in the heat flux at other points on a vehicle. From the previous discussion of heat-flux distribution it will be recalled that the radiative heat flux is at much lower levels at points away from the stagnation point than is the convective. Thus for the complete nose, the ratio of total radiative to convective heat will be less than that indicated by the total heat values presented for the stagnation point.

In any final assessment of the heating problem for a particular vehicle one has to consider the heating of surfaces of the vehicle other than the nose, other heating conditions, and the reaction of the heat

shield. Other surfaces that require attention are the afterbody, the base, and any control surfaces. Other heating conditions are nonequilibrium radiative and convective heating, both in the shock layer and the wake, and radiative heating resulting from ablation products entrained in the shock layer and the wake. These aspects of the entry heating problem are beyond the scope of this paper. It must be remarked, however, that an assessment of the relative importance of the two types of heating on the basis of the total heat load can be very misleading if the efficiency of the heat protection system is greatly different for the two types of heating.

6. CONCLUDING REMARKS

This paper has considered the problem of predicting the equilibrium radiative heating of vehicles entering the Earth's atmosphere at velocities up to twice satellite velocity. It was shown that there are four conditions of equilibrium radiative heating of general concern. These are (1) no decay or absorption, (2) decay, (3) absorption and, (4) decay and absorption. The velocity-altitude boundaries for each condition were shown to be functions of vehicle size.

Stagnation-point radiative heating for the condition of no decay or absorption was shown to be amenable to rapid calculation for spherical segment noses. The radiative heat flux bears the well-known direct proportionality to nose radius by virtue of the direct proportionality between nose radius and shock standoff distance. It was noted that the accuracy of the calculations are subject to some uncertainty for velocities approaching twice satellite velocity.

Radiative heat-flux distributions were presented for spherical segment noses for wide ranges of velocity and altitude. The effects of these two variables on the distributions were minor. The radiative heat flux decreases much more rapidly at points away from the stagnation point than does convective heat flux.

Results for the cases of either decay or absorption or both are presently limited to one-dimensional flow. Examples of the results were examined for two combinations of velocity and altitude; one for which only decay was important, and the other for which both decay and absorption were important. Sizable reductions in radiative heat flux were noted. It is believed, however, that the effects of decay and absorption will not be very significant for manned vehicles entering the atmosphere at velocities up to twice satellite velocity.

Comparisons of stagnation-point radiative and convective heat flux for manned vehicles returning to Earth from trips to the Moon and to Mars showed the anticipated effect of increasing entry velocity. The peak radiative heat flux changed from a less dominant to a dominant level relative to the peak convective heat flux. This was the result of a twentyfold increase in the radiative peak compared to only a twofold increase in the convective peak. From the standpoint of total heat for the stagnation region, the two types of heating were of equal importance for the Mars vehicle. This is in contrast to the situation for the lunar vehicle for which the radiative total heat was about 5 percent of the convective. The combined total heat for the Mars vehicle was about four times that for the lunar vehicle. Thus manned vehicles for entry from trips to Mars present a much greater challenge to heat-shield designers than vehicles returning from the Moon.

REFERENCES

1. Canning, Thomas N., and Page, William A.: Measurements of Radiation From Flow Fields of Bodies Flying at Speeds Up to 13.4 Kilometers Per Second. Paper presented to the Fluid Mechanics Panel of AGARD, Brussels, Belgium, April 3-6, 1962.

2. Kivel, B., and Bailey, K.: Tables of Radiation from High Temperature Air. Res. Rep. 21, AVCO Res. Lab., Dec. 1957.

3. Kivel, Bennett: Radiation from Hot Air and Stagnation Heating. Rep. 79, AVCO-Everett Res. Lab., Oct. 1959.

4. Meyerott, R. E., Sokoloff, J., and Nicholls, R. W.: Absorption Coefficients of Air. LMSD 288052, Lockheed Aircraft Corp., July 1960.

5. Kaattari, George E.: Predicted Shock Envelopes About Two Types of Vehicles at Large Angles of Attack. NASA TN D-860, 1961.

6. Yoshikawa, Kenneth K., and Wick, Bradford H.: Radiative Heat Transfer During Atmosphere Entry at Parabolic Velocity. NASA TN D-1074, 1961.

7. de l'Estoile, H., and Rosenthal, L.: Rapid Evaluation of Radiant Heating During Re-Entry into the Atmosphere. Aero. and Astro. Proc. of the Durand Centennial Conf., ed. by N. J. Hoff and W. G. Vincenti, Pergamon Press, N. Y., 1960, pp. 173 - 203.

8. Hochstim, Adolf R.: Gas Properties Behind Shocks at Hypersonic Velocities. I. Normal Shocks in Air. Rep. No. ZPh (GP)-002, CONVAIR, Jan. 30, 1957.

9. Maslen, S. H., and Moeckel, W. E.: Inviscid Hypersonic Flow Past Blunt Bodies. Jour. Aero. Sci., vol. 24, no. 9, Sept. 1957, pp. 683 - 693.

10. Fuller, Franklin B.: Numerical Solutions for Supersonic Flow of an Ideal Gas Around Blunt Two-Dimensional Bodies. NASA TN D-791, 1961.

11. Goulard, R., and Goulard M.: Energy Transfer in the Couette Flow of a Radiant and Chemically Reacting Gas. Heat Transfer and Fluid Mechanics Inst., 1959.

12. Goulard, R., and Goulard, M.: One Dimensional Energy Transfer in Radiant Media. Int'l. Jour. Heat Mass Transfer, vol. 1, Pergamon Press, June 1960, pp. 81 - 91.

13. Kourganoff, V.: Basic Methods in Transfer Problems. Clarendon Press, Oxford, 1952.

14. Chandrasekhar, S.: Radiative Transfer. Clarendon Press, Oxford, 1950.

15. Goulard, R.: The Coupling of Radiation and Convection in Detached Shock Layers. Bendix Product Div., Applied Sciences Lab., Apr. 1959.

16. Goulard, R.: A Comment on "Radiation from Hot Air and Its Effect on Stagnation-Point Heating." Readers' Forum, Jour. of Aerospace Sci., vol. 28, no. 2, Feb. 1961, pp. 158 - 159.

17. Kennet, H., and Strack, S. L.: Stagnation Point Radiative Transfer. Technical Note, ARS Jour., vol. 31, no. 3, March 1961, pp. 370 - 372.

18. Adams, Mac C.: A Look at the Heat Transfer Problem at Super Satellite Speeds. ARS Preprint 1556-60, American Rocket Soc., Dec. 1960.

19. Chapman, Dean R.: An Analysis of the Corridor and Guidance Requirements for Supercircular Entry into Planetary Atmospheres. NASA TR R-55, 1960.

20. Lees, Lester: Recovery Dynamics - Heat Transfer at Hypersonic Speeds in a Planetary Atmosphere. Space Technology, Ch. 12, Howard Seifert, ed., John Wiley and Sons, New York, 1959, pp. 12-01 to 12-20.

21. Traugott, Stephen C.: An Approximate Solution of the Direct Supersonic Blunt-Body Problem for Arbitrary Axisymmetric Shapes. Jour. of the Aerospace Sci., vol. 27, no. 5, May 1960, pp. 361 - 370.

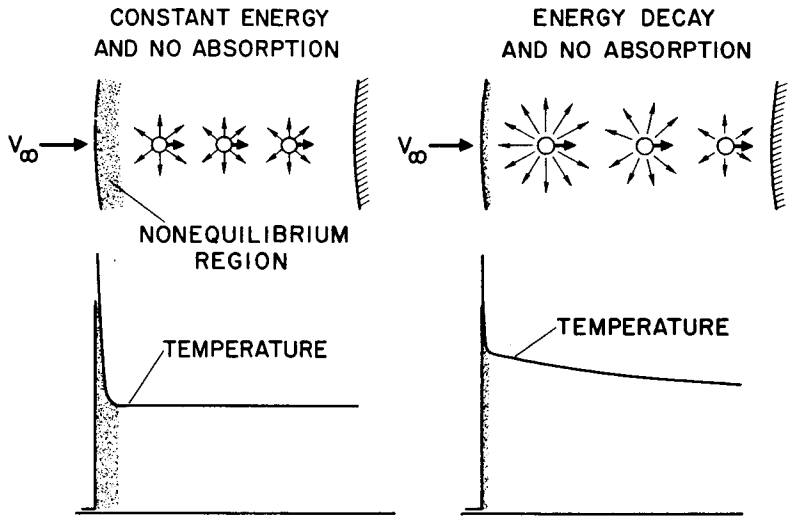

Fig. 1.- Shock layers for equilibrium radiative heating.

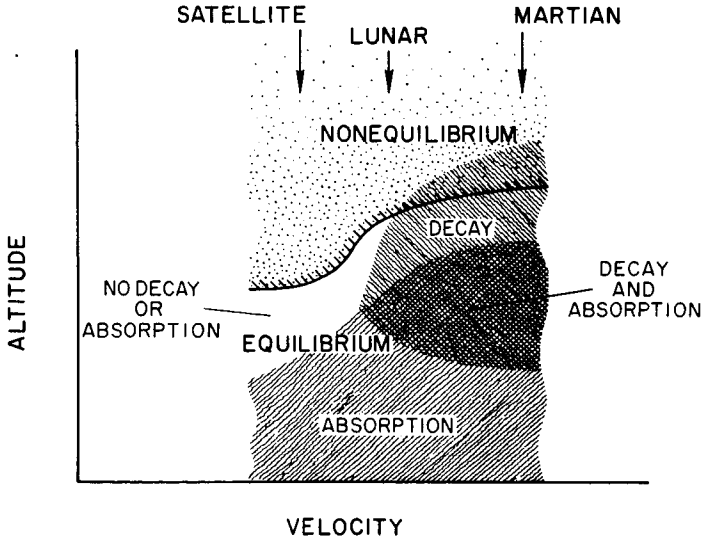

Fig. 2.- Important altitude-velocity regions.

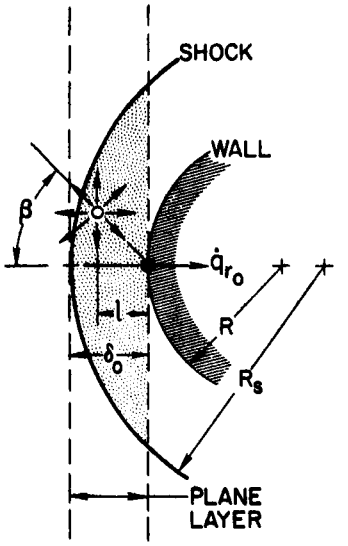

PLANE LAYER:

$$\dot{q}_{r_o} = (E_t/2)\delta_o \int_0^{\pi/2} \int_0^{1} \sin\beta \, d(l/\delta_o) d\beta$$

$$= (E_t/2)\delta_o$$

SHOCK LAYER:

$$\dot{q}_{r_o} = (E_t/2)\delta_o \int_0^{\pi/2} \int_0^{l_s/\delta_o} \sin\beta \, d(l/\delta_o) d\beta$$

$$= (E_t/2)\delta_o k_s$$

Fig. 3.- Stagnation-point flux from a constant-energy layer without absorption.

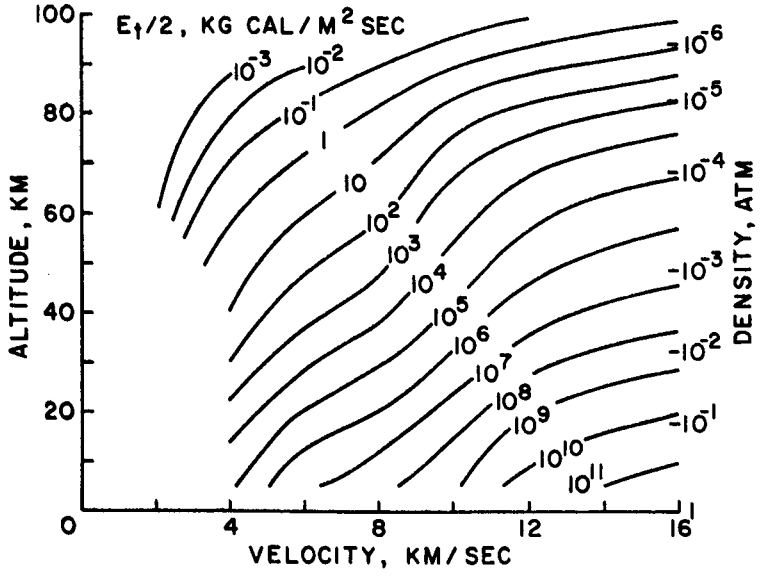

Fig. 4.- Equilibrium radiant energy.

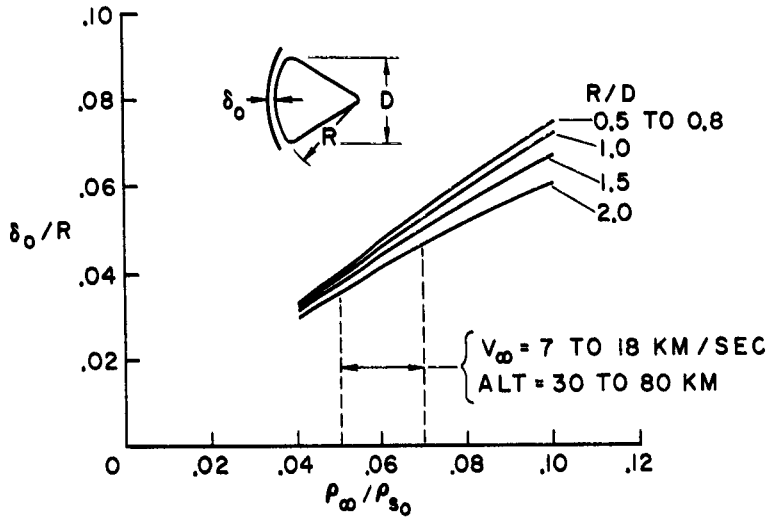

Fig. 5.- Shock standoff for zero angle of attack.

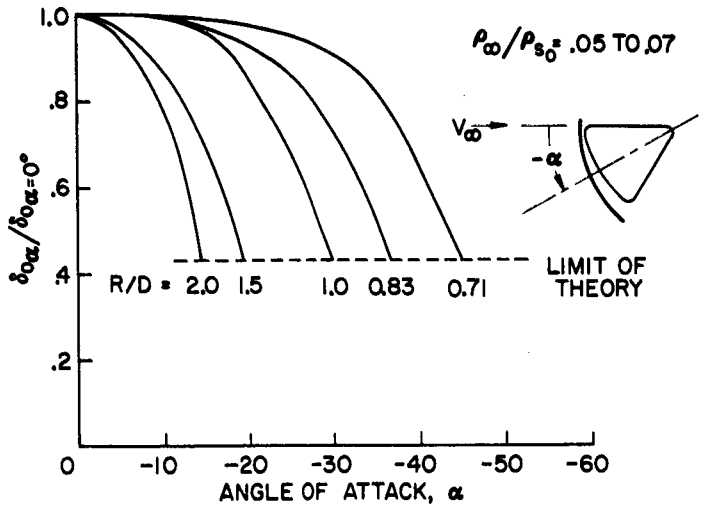

Fig. 6.- Effect of angle of attack on shock standoff.

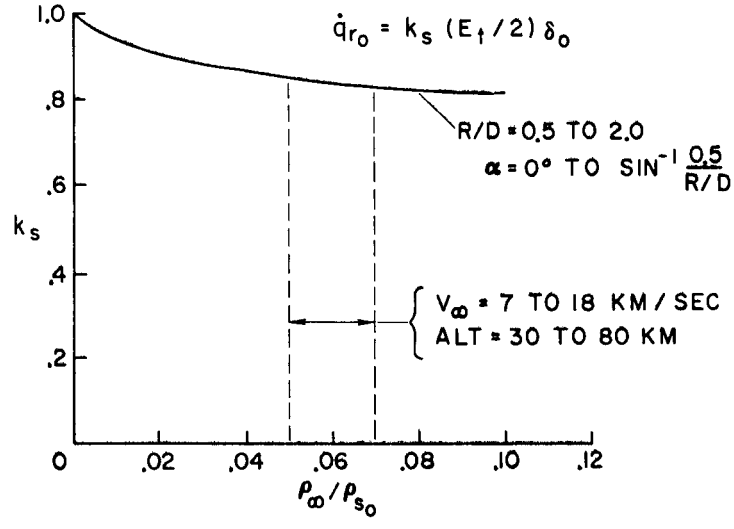

Fig. 7.- Shape factor for stagnation-point flux.

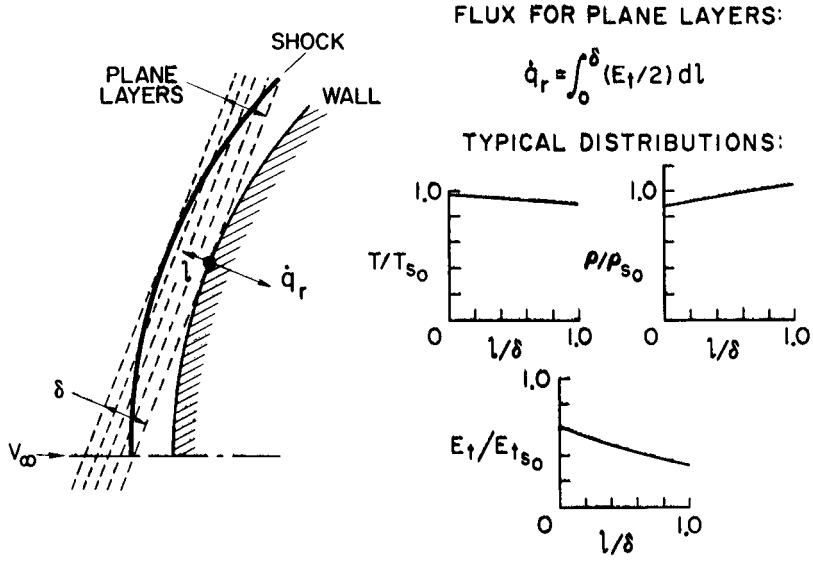

Fig. 8.- Flux from a constant-energy layer without absorption.

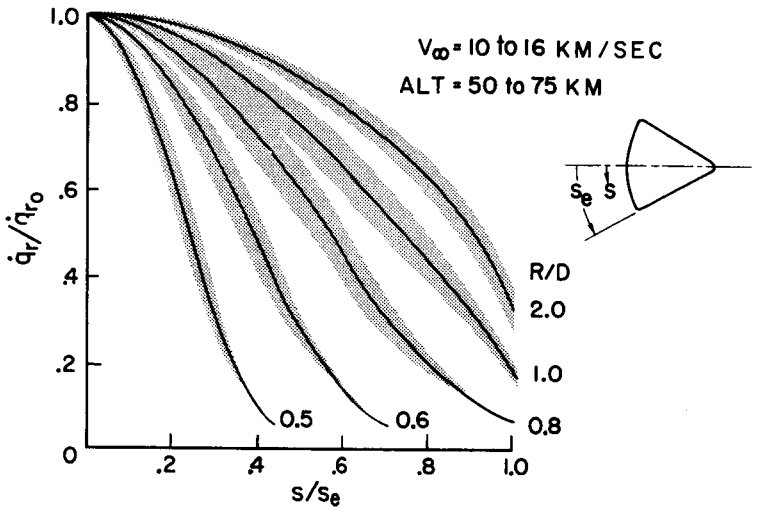

Fig. 9.- Radiative flux distributions at zero angle of attack.

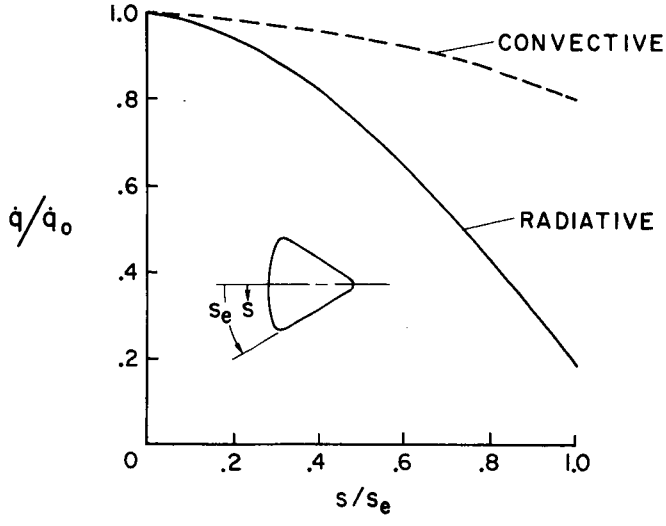

Fig. 10.- Radiative and laminar convective heat flux distributions at zero angle of attack; R/D = 1.0.

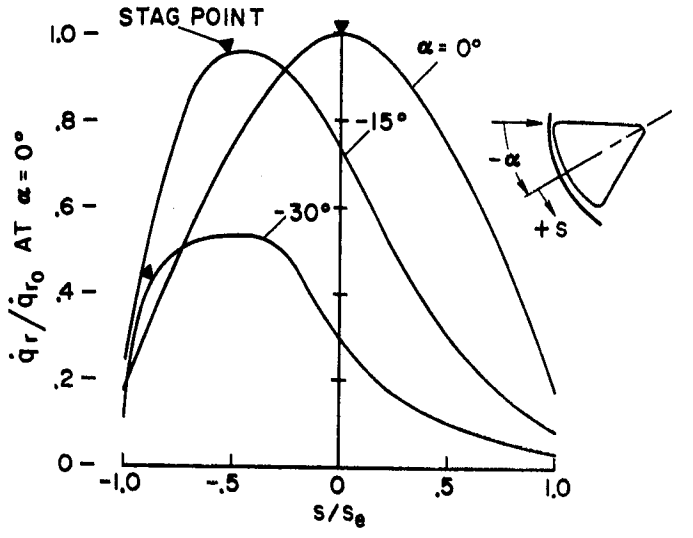

Fig. 11.- Radiative flux distributions at angle of attack; R/D = 1.0.

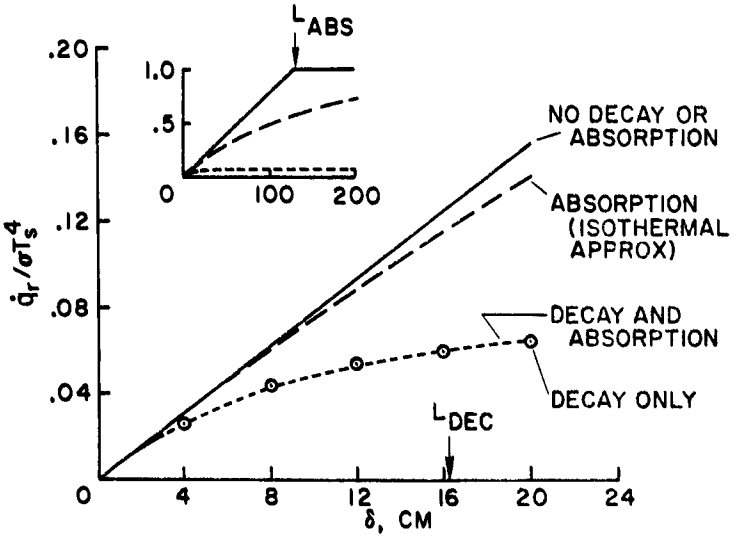

Fig. 12.- Effect of decay and absorption; V_∞ = 15 km/sec, Altitude = 57 km.

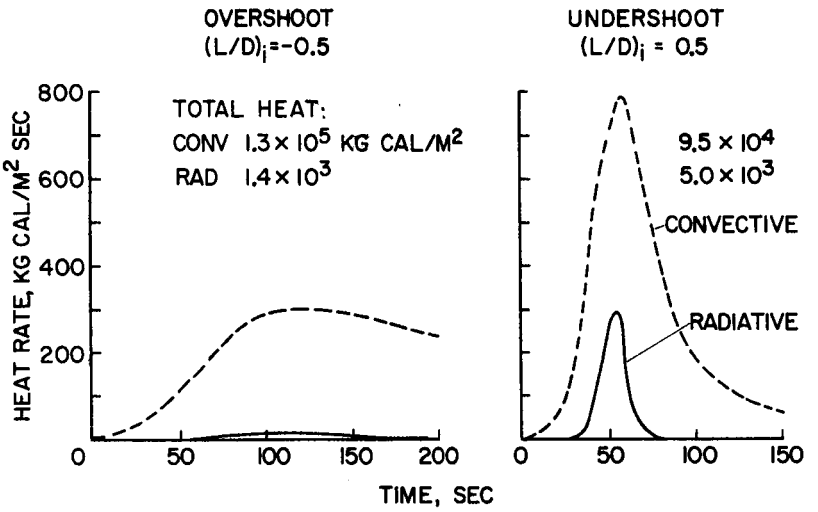

Fig. 13.- Entry heating for a manned lunar vehicle; W/C_DA = 250 kg/m^2; R = 3m.

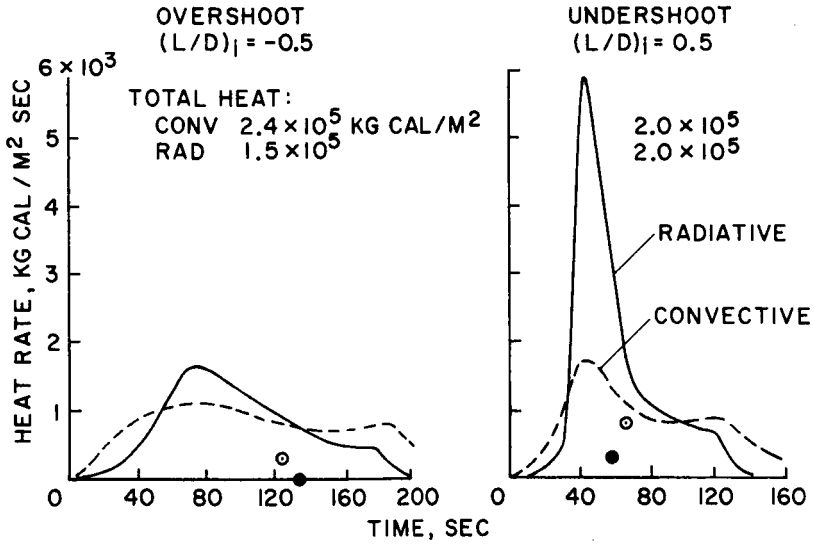

Fig. 14.- Entry heating for a manned vehicle returning from Mars; W/C_DA = 250 kg/m^2; R = 3m.